ELSEVIER

Contents lists available at ScienceDirect

Journal of Hydrology

journal homepage: www.elsevier.com/locate/jhydrol



Research papers



Estimating soil water retention curves over the entire saturation range: A thermal conductivity-based approach

Yongwei Fu^{a,b,c}, Robert Horton^d, Joshua Heitman^{c,*}

- a College of Land Science and Technology, China Agricultural University, Beijing, China
- b Key Laboratory of Arable Land Conservation in North China, Ministry of Agriculture and Rural Affairs, Beijing, China
- ^c Department of Crop and Soil Sciences, North Carolina State University, Raleigh, United States
- d Department of Agronomy, Iowa State University, Ames, United States

ARTICLE INFO

This manuscript was handled by Corrado Corradini, Editor-in-Chief, with the assistance of Simone Di Prima, Associate Editor

Keywords:
Soil water retention curve
Thermal conductivity
Hydraulic continuity
Capillarity
Adsorption

ABSTRACT

The relationship between soil water content (θ) and suction (h, referring to the absolute value of pressure head), is described by the soil water retention curve (SWRC). Our earlier research (Fu et al. (2021, 2023a) [J. Hydrol.127171]; [J. Hydrol.129898]) recognized underlying correlations between SWRCs and soil thermal conductivity (λ) versus θ curves, and developed methodologies to ascertain the parameters of the van Genuchten (vG) equation using $\lambda(\theta)$ measurements, described by the Ghanbarian & Daigle (GD) equation, and basic soil characteristics. Limitations intrinsic to the van Genuchten equation restrict the GD-vG approach to generate precise estimates only in the wet and medium suction range, specifically h ranging from 0 to 150 mH₂O. The validity of these approaches in the dry region remains uncertain. In this study, we associated the Peters-Durner-Iden (PDI) model parameters to those of the GD model. An initial examination was performed on the linearization processes needed to derive the hydraulic continuity water content (θ_{hc}) from the capillary water component as characterized by the PDI model and to choose the suction at oven dryness (h_0) based on PDI model performance. Subsequently, two piecewise functions and two pedo-transfer functions were formulated to compute the PDI model parameters utilizing soil porosity, particle size distribution, and GD parameters, based on a calibration dataset comprising 25 different soils. The new GD-PDI approach was subsequently assessed with six independent soils and juxtaposed with the previous GD-vG approach. The GD-PDI approach outperformed the GD-vG approach, particularly within the dry range.

1. Introduction

Understanding the behavior of water in unsaturated porous media poses a significant challenge for vadose zone studies. To accurately describe water behavior in unsaturated soils, it is crucial to obtain accurate estimates of soil water retention functions. The soil water retention curve (SWRC) describes the relationship between suction (h, also the absolute of pressure head) and soil water content (θ).

Various analytical functions to describe the SWRC can be found in the literature (Brooks and Corey, 1964; van Genuchten, 1980; Kosugi, 1994). Most of them mainly account for water held in capillary spaces and not water films adsorbed to solid surfaces. Consequently, while they accurately represent the SWRC in the medium to wet moisture range, they fail to describe the observed trend in the dry region. Over the past three decades, numerous attempts have been made to obtain a complete

retention curve over the entire moisture range (Ross et al., 1991; Campbell and Shiozawa, 1992; Rossi and Nimmo, 1994; Fayer and Simmons, 1995; Webb, 2000; Groenevelt and Grant, 2004; Khlosi et al., 2006; Zhang, 2011). However, existing models, such as those proposed by Fayer and Simmons (1995), Khlosi et al. (2006), and Zhang (2011), frequently fall short in achieving zero water content particularly when dealing with soils that have a wide range of pore sizes (Peters, 2013). In recent years, the Peters-Durner-Iden (PDI) model system has emerged as a successful option. Initially introduced by Peters (2013) and subsequently refined by Iden and Durner (2014), this model has demonstrated its effectiveness in accurately describing the entire soil water retention curve (SWRC) from saturation to oven dryness, and for simulating water redistribution in desert soil (Luo et al., 2020; Peters et al., 2021; Peters et al., 2023).

Direct measurements of SWRCs can be challenging and time-

E-mail address: jlheitman@ncsu.edu (J. Heitman).

 $^{^{\}ast}$ Corresponding author.

consuming, especially when considering larger spatial scales (Zhang et al., 2018; Dai et al., 2019). To overcome this limitation, pedo-transfer functions (PTFs) have been developed, which estimate SWRC-model parameters using available soil property values such as soil texture, bulk density, and organic carbon content (Van Looy et al., 2017). Machine learning algorithms, including artificial neural network (Zhang and Schaap, 2017; Rudiyanto et al., 2021), random forests (Wang et al., 2022) and regression method (Weber et al., 2020), have been increasingly employed to build modern PTFs, offering improved capacity to handle the non-linear relationships and complexity between predictors and target values. However, the reliability of PTFs is uncertain and requires careful validation when applied to regions or conditions beyond their original development. Furthermore, it is increasingly recognized that current PTFs do not explicitly account for pedological properties, soil structure, temporal variations, and climate influences which also affect soil hydraulic properties (Vereecken et al., 2022; Weber et al., 2024).

Connections between soil thermal conductivity (λ) versus water content (θ) curves and soil water retention curves have been studied. Earlier research has identified distinct regions within $\lambda(\theta)$ curves with bound water content values also playing a crucial role in determining soil hydraulic properties, as indicated by SWRCs (Tarnawski and Gori, 2002; Lu and Dong, 2015). Fu et al. (2021a) proposed a parametric method to estimate SWRCs from measured $\lambda(\theta)$ values and basic soil parameters. However, this method has limitations near saturation due to the Lu and Dong (2015) model assumptions on which it was based. The Ghanbarian and Daigle (GD) model was developed using a combination of percolation theory and effective medium approximation to effectively describe variations in λ with θ across a range from saturation to oven dryness (Ghanbarian and Daigle, 2016). Building upon this work, Fu et al. (2023b) investigated the inherent correlation between $\lambda(\theta)$ curves and SWRCs using GD and van Genuchten (vG) models, respectively. They established relationships between GD model parameters and several important water content values, such as residual water content, water content at the SWRC inflection point, and the hydraulic continuity water content estimated from a SWRC. They concluded that strong correlations observed between these model parameters can be attributed to an intrinsic correlation between heat transfer and water retention mechanisms. Furthermore, Fu et al. (2023a) developed approaches to estimate the van Genuchten model parameters based on $\lambda(\theta)$ measurements described by the GD model. Although yielding satisfactory results on independent validation, their applicability in the dry range is questionable due to the limitations of the vG model, as discussed earlier.

The aim of this study is to propose a novel method to estimate a complete SWRC using $\lambda(\theta)$ measurements. The PDI and GD models are employed as they have the capability to accurately depict entire SWRCs and $\lambda(\theta)$ curves from saturation to oven dryness. A newly developed GD-PDI approach is established using a calibration dataset comprising 25 different soil samples, and it is subsequently validated using an additional six independent soils.

2. Theory

2.1. GD-vG approach

Heat transfer and water retention in soils, governed in part by soil thermal conductivity (λ) and water retention curves, are coupled. Fu et al. (2023b) investigated the intrinsic correlation between $\lambda(\theta)$ and SWRC using the GD and vG models. The GD model includes two parameters: scaling exponent t_s and critical water content θ_c and its details are provided in Appendix A. The vG model is expressed as,

$$\frac{\theta - \theta_{\rm r}}{\theta_{\rm s} - \theta_{\rm r}} = \left[1 + (\alpha \ h)^n\right]^{(1/n - 1)} \tag{1}$$

where θ_s and θ_r are saturated and residual water content (m³ m⁻³),

respectively. α and n (>1) are parameters in the vG model.

Using 20 soils from the literature, Fu et al. (2023a) linked critical water content θ_c to pore size distribution parameter n and found a strong logarithmic correlation between them as follows:

$$\frac{1}{n} = 0.2721 \ln(\theta_c) + 1.3904 \tag{2}$$

Eq. [2] is consistent with previous studies in which the critical water content θ_c was reported to be closely related to soil clay content: with increasing clay content, θ_c increases (Ghanbarian and Daigle, 2016; Fu et al., 2023c). The pore size distribution parameter n, which is used as a surrogate for "soil coarseness", is also a function of clay content (Lehmann et al., 2020; Rudiyanto et al., 2021). Coarser soils have a relatively narrow pore size distribution, and generally have relatively large values of n (Carsel and Parrish, 1988).

Fu et al. (2023a) also established a strong correlation (R^2 of 0.94) between critical water content θ_c and hydraulic continuity water content (θ_{hc}) as follows:

$$\theta_{hc} = 0.1046 ln(\theta_c) + 0.5464 \tag{3}$$

The justification of Eq. [3] can be attributed to the intrinsic correlation between heat transfer and water flow processes as θ_{hc} indicates a critical water content where capillary-driven hydraulic continuity is disrupted (Lehmann et al., 2008). At θ values larger than θ_{hc} , λ increases mainly due to capillary water replacing air bubbles in the pore space, and thus as water content increases the rate of λ increases gradually decrease (Fu et al., 2023b). θ_{hc} can be estimated from a SWRC with fitted vG model parameters as follows:

$$\theta_{\rm hc} = (\theta_{\rm s} - \theta_{\rm r}) \left[1 + \left(\frac{n-1}{n} \right)^{1-2n} \right]^{\frac{1-n}{n}} + \theta_{\rm r} \tag{4}$$

Detailed derivation steps of Eq. [4] are provided in Appendix B.

Fu et al. (2023a) presented the following equations to estimate vG model parameters θ_s and α from soil property values and GD model parameters:

$$\theta_{s} = \phi$$
 (5)

$$ln(\alpha) = 4.03 + 1.07 f_{sand} - 8.31 f_{clay} - 14.55 \phi - 1.16 \lambda_{sat} + 0.19 t_s + 29.69 \theta_c$$
(6)

where $f_{\rm sand}$ (g g⁻¹), $f_{\rm clay}$ (g g⁻¹), ϕ , and $\lambda_{\rm sat}$ (W m⁻² K⁻¹) are sand content, clay content, porosity, and saturated thermal conductivity, respectively.

In summary, Fu et al. (2023a) introduced an approach, referred to as the GD-vG approach, to estimate the vG parameters from $\lambda(\theta)$ measurements and basic soil properties (i.e., particle size distribution and porosity). This approach involves several steps: First, θ_c and t_s values are determined by fitting the GD model to measured $\lambda(\theta)$ values; Next, n, θ_{hc} , θ_s and α are estimated using Eqs. [2], [3], [5] and [6], respectively; Finally, θ_r is calculated from Eq. [4] once the values of n and θ_s are known.

2.2. Hydraulic continuity water content estimated with the Peters-Durner-Iden model

The hydraulic continuity water content (θ_{hc} in Eqs. [3] and [4]) is associated with the suction at which the hydraulically connected thick liquid films within the soil pore space are disrupted and stage-I soil water evaporation (i.e., a high and relatively constant evaporation rate supported by capillary flow to the surface) cannot be maintained (Lehmann et al., 2008; Assouline et al., 2014). The spatial extent of the film region depends on capillary pressure forces driving liquid flow from a receding drying front to the soil surface. Lehmann et al. (2008)

assumed that the capillary pressure required for draining the largest and smallest drainable pores in this "active" range can be represented by the air-entry suction (ha) and the suction at which hydraulic continuity for capillary flow is interrupted (h_{hc}), respectively. The assumption is justified as the vG model can accurately describe the SWRC within the capillary regime which mainly depends on the pore size distribution. Previous studies reported that h_a can be approximated from the intersection of the tangent line drawn across the inflection point of a SWRC and a horizontal line drawn at θ_s (Fredlund and Xing, 1994; Zhai and Rahardjo, 2012; Fu et al., 2021b). Then $h_{\rm hc}$ can be computed symmetrically as the intersection of the tangent line and a horizontal line drawn across the inflection point and $\boldsymbol{\theta}_r$ modeled by the vG model, respectively (Fig. 1a). However, each soil has a unique maximum h value at which water content approaches zero (Zhang et al., 2017), marking the concept of θ_r as being inappropriate. Additionally, previous studies also find that unconstrained curve fitting can produce non-physical negative θ_r values (Groenevelt and Grant, 2004; Haverkamp et al., 2005), which inevitably yield unreliable θ_{hc} estimates from Eq. [4].

Water retention in soils is controlled by two mechanisms: capillarity and adsorption, which depend on pore size distribution, mineral surface and composition, respectively (Lu, 2016). At a fixed h value, capillary water and adsorbed water coexist within the soil. These two types of water vary in their quantities and contribute independently to the soil's overall water content. The linearization method presented in Lehmann et al. (2008) is proposed to estimate the characteristic length supporting capillary-driven liquid flow, which is mainly determined by the width of the pore size distribution. Thus, linearization procedures need to be conducted on the capillary water component only, rather than on the complete SWRC. However, the vG equation does not explicitly distinguish between adsorption and capillary water within the SWRC curve. Considering the limitations regarding the vG model discussed above, Fu et al. (2023a, 2023b) used SWRC data from 0 to 150 mH₂O to determine vG model parameters before calculating θ_{hc} . This pragmatic constraint gave good model performance for the conditions tested, but also limited the applicability of the GD-vG approach to estimate the SWRC over the complete saturation range. To address this limitation, we adopt the Peters-Durner-Iden (PDI) model here as it can describe the full SWRC from saturation to oven dryness well and distinguish the capillary and adsorption water components.

A brief review of the PDI water retention model is provided in Appendix C and more details can be found in Peters et al. (2023). In the following, we will show the derivation to deduce the hydraulic continuity water content estimated from the PDI model using the full SWRC data from saturation to dry. The graphical linearization details are

provided in Fig. 1b. The capillary water component (θ_{cap}) in the PDI water retention model can be obtained by combining Eqs. [C1]-[C3],

$$\theta_{\text{cap}} = (\theta_{\text{s}} - \theta_{\text{r}}) \frac{\left[1 + (\alpha \ h)^{n}\right]^{(1/n-1)} - \left[1 + (\alpha \ h_{0})^{n}\right]^{(1/n-1)}}{1 - \left[1 + (\alpha \ h_{0})^{n}\right]^{(1/n-1)}} \tag{7}$$

where h_0 is the suction at oven dryness. The first and second derivatives of Eq. [7] with respect to h are therefore described as,

$$\frac{d\theta_{\text{cap}}}{dh} = (\theta_{\text{s}} - \theta_{\text{r}}) \frac{(-n+1)\alpha^{n}h^{n-1}[1 + (\alpha \ h)^{n}]^{(-2+1/n)}}{1 - [1 + (\alpha \ h_{0})^{n}]^{(1/n-1)}}$$
(8)

$$\frac{d^{2}\theta_{\text{cap}}}{dh^{2}} = \frac{(\theta_{s} - \theta_{r})(-n+1)\alpha^{n}h^{n-2}[1 + (\alpha \ h)^{n}]^{(-3+1/n)}\{1 + n[(\alpha \ h)^{n} - 1]\}}{1 - [1 + (\alpha \ h_{0})^{n}]^{(1/n-1)}}$$
(9)

An analogous expression for Eq. [B3] is thus obtained by solving $\frac{d^2\theta_c}{dh^2}=0,$

$$h_{\rm i}^* = \frac{1}{\alpha} \left(1 - \frac{1}{n} \right)^{1/n}$$
 (10)

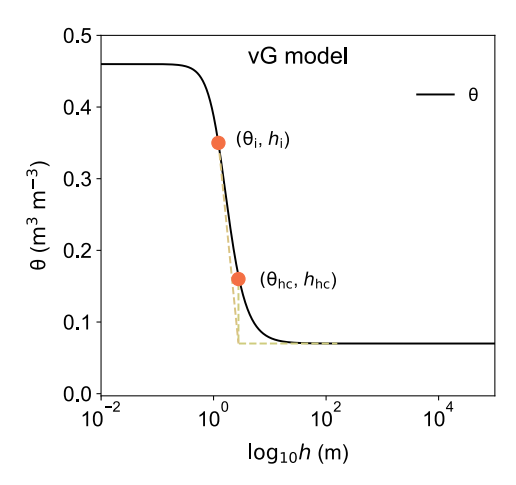
where h^* i is the suction at the inflection point of the capillary water component. Substituting h^* i from Eq. [10] into Eq. [7] yields,

$$\theta_{i-cap} = (\theta_s - \theta_r) \frac{\left(2 - \frac{1}{n}\right)^{-1 + 1/n} - \left[1 + (\alpha \ h_0)^n\right]^{(1/n - 1)}}{1 - \left[1 + (\alpha \ h_0)^n\right]^{(1/n - 1)}}$$
(11)

where $\theta_{i\text{-}cap}$ is the water content at the inflection point of the capillary water component and its corresponding slope (i.e., first derivative) is expressed as

$$\left[\frac{d\theta_{\text{cap}}}{dh}\right]_{h=h_{i}^{*}} = \frac{(\theta_{s}-\theta_{r})(-n+1)\alpha\left(1-\frac{1}{n}\right)^{(1-1/n)}\left(2-\frac{1}{n}\right)^{(-2+1/n)}}{1-\left[1+\left(\alpha\ h_{0}\right)^{n}\right]^{(1/n-1)}} \tag{12}$$

We first draw a tangent line at the inflection point (h^* i, $\theta_{i\text{-cap}}$) using the slope from Eq. [12], which then intersects with a horizontal line drawn across θ_r (= 0 for the capillary water retention component as shown in Fig. 1b). The intersection point of these lines marks the suction which is synonymous to the hydraulic continuity suction (h^* hc) for the PDI model, as



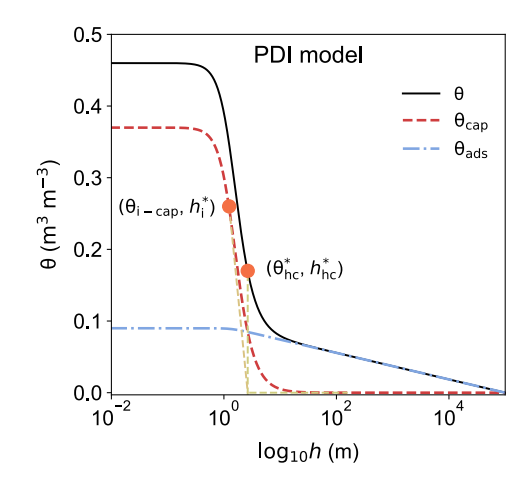


Fig. 1. Linearization method to determine the hydraulic continuity water content based on the van Genuchten (vG) model and Peters-Durner-Iden (PDI) model for Soil 2 in this study. Fitted parameters are: $\theta_s = 0.46 \text{ m3/m}^{-3}(-|-)$, $\theta_r = 0.07 \text{ m3/m}^{-3}(-|-)$, $\alpha = 0.71 \text{ m}^{-1}$ and n = 2.97 (dimensionless) for the vG model; $\theta_s = 0.46 \text{ m3/m}^{-3}(-|-)$, $\theta_r = 0.09 \text{ m3/m}^{-3}(-|-)$, respectively.

$$h_{\rm hc}^* = \frac{\left(2 - \frac{1}{n}\right)^{-1 + 1/n} - \left[1 + \left(\alpha \ h_0\right)^n\right]^{(1/n - 1)}}{(n - 1)\alpha \left(1 - \frac{1}{n}\right)^{(1 - 1/n)} \left(2 - \frac{1}{n}\right)^{(-2 + 1/n)}} + \frac{1}{\alpha} \left(1 - \frac{1}{n}\right)^{1/n} \tag{13}$$

Substituting Equation [13] into the PDI model (refer to Appendix C) allows for the expression of the hydraulic continuity water content (θ^* hc) in relation to the parameters of the PDI model (θ_s , θ_r , α , n, and h_0). Owing to its intricate nature, we refrain from providing an explicit expression in this context. However, we do provide a Python code to facilitate its computation.

2.3. A new approach to estimate a complete full range SWRC from $\lambda(\theta)$ data

As discussed above, the GD-vG approach was established using SWRC data only from h values of 0 to 150 mH₂O. If one relates $\theta_{\rm c}$ to θ^{\star} hc, and n is estimated from the PDI model fitted to the complete SWRC dataset, the following piecewise linear equations between θ^{\star} hc and 1/n with $\theta_{\rm c}$ are proposed,

$$1/n = a_1 \theta_c + a_2 \quad \theta_c \le \theta_1 \tag{14a}$$

$$1/n = a_3\theta_c + a_4 \quad \theta_c > \theta \tag{14b}$$

$$\theta_{\mathrm{hc}}^* = f(\theta_{\mathrm{s}}, \theta_{\mathrm{r}}, \alpha, n, h_0) = b_1 \theta_{\mathrm{c}} + b_2 \quad \theta_{\mathrm{c}} \le \theta_2 \tag{15a}$$

$$\theta_{\rm hc}^* = f(\theta_{\rm s}, \theta_{\rm r}, \alpha, n, h_0) = b_3 \theta_{\rm c} + b_4 \quad \theta_{\rm c} > \theta_2 \tag{15b}$$

where a and b are empirical parameters, and θ_1 and θ_2 are threshold water contents

The Eq. [5] assumption that θ_s is equal to porosity does not hold for most soils. For field soils, repeated wetting–drying cycles often leads to a quasi-saturated condition, characterized by the existence of entrapped air in the pores of a water-saturated soil. As a result, θ_s values are typically smaller than the porosity (Fayer and Hillel, 1986). Therefore, we construct the following function to estimate θ_s :

$$\theta_{\rm s} = c_1 + c_2 f_{\rm sand} + c_3 \phi \tag{16}$$

where the c-terms are empirical coefficients. Obviously, c_3 must be close but slightly smaller than unity because of the strong correlation between θ_s and ϕ . Sand content is used as a predictor accounting for the influence of texture.

An analogous pedo-transfer function to Eq. [6] is established,

$$\ln(\alpha) = d_1 + d_2 f_{\text{clav}} + d_3 \phi + d_4 \ln(\lambda_{\text{sat}}) + d_5 \theta_c$$
(17)

where d-terms are empirical coefficients. Two important facts regarding Eq. [17] need be highlighted. First, a reduced number of predictors are used in comparison to Eq. [6] to augment the robustness and universality of the model. Second, the natural logarithm of $\lambda_{\rm sat}$ is employed due to its significantly greater magnitude relative to the other predictive factors.

The calibration of the above equations follows these steps. First, the GD and PDI models, respectively, are fitted to the measured $\lambda(\theta)$ and SWRC data to obtain their respective model parameters. Then, θ^* hc is estimated from PDI model parameters (θ_s , θ_r , α , n) following steps outlined in section 3.3. Subsequently, the coefficients in Eqs. [14]-[17] are determined using the known values of θ_c , t_s , θ^* hc and n obtained in the prior steps. Once these steps are completed, a new approach to estimate the complete full range SWRC from $\lambda(\theta)$ measurements is developed.

3. Materials and methods

We compiled a dataset consisting of 31 soil samples from the literature, including 25 for model calibration and 6 for model validation. The

SWRC data cover a h range of 0 to 10^5 m, and the $\lambda(\theta)$ data span from dry to saturation. Soils 1–25 were chosen as the calibration dataset to represent a diverse range of soil properties. These soils exhibited varying textures, with sand content ranging from 0.09 to 1 g g⁻¹ and clay content ranging from 0 to 0.54 g g⁻¹. Additionally, they had varying quartz content, ranging from 0.12 to 1 g g⁻¹, and porosity values, which range from 0.32 to 0.60 m³ m⁻³. A summary of these soil characteristics can be found in Table 1. The validation dataset, consisting of Soils 26–31, is consistent with that of Fu et al. (2023a) to streamline the comparative analysis. Apart from the available $\theta(h)$ and $\lambda(\theta)$ datasets, the selected soils in the validation dataset were constrained by the requirement that soil properties such as bulk density, particle density and soil texture were known, because they are required inputs for the GD-vG approach (Table 2).

The GD model requires a dry soil thermal conductivity value (λ_{dry}) and λ_{sat} as input parameters. For soils without λ_{dry} and λ_{sat} measurements (Soils 1–5, 15 and 16), values were estimated using the following empirical functions of Lu et al. (2007) and Johansen (1975),

$$\lambda_{dry} = -0.56\phi + 0.51\tag{18}$$

$$\lambda_{\text{sat}} = \lambda_{\text{s}}^{1-\phi} \lambda_{\text{w}}^{\phi} = \left(\lambda_{\text{q}}^{f_{\text{q}}} \lambda_{\text{o}}^{1-f_{\text{q}}}\right)^{1-\phi} \lambda_{\text{w}}^{\phi} \tag{19}$$

where λ_s , λ_q , λ_o , and λ_w are thermal conductivities of soil solids, quartz (7.7 W/m K⁻¹), other minerals, and water (0.56 W/m K⁻¹), respectively; and f_q is the volumetric fraction of quartz, which can be assumed as being equal to the mass fraction of quartz (reported in Table 1) as most soil minerals have density values similar to 2.65 Mg m⁻³ (Tarnawski et al., 2015). The value for λ_o is taken as 2.0 W/m K⁻¹ for soils with $f_q > 0.2$, and 3.0 W/m K⁻¹ for soils with $f_q \le 0.2$ (Johansen, 1975). A comprehensive review of Eqs. [18] and [19] has been provided in previous studies (He et al., 2021; Fu et al., 2023c, 2023d), and thus it is not addressed again here.

4. Results and discussion

4.1. Uncertainty from variation in h_0

The suction at oven dryness h_0 is commonly set to 10^5 m as the endpoint at the intersection with the y-axis to describe the SWRC $(\theta(h))$ under dry conditions (Ross et al., 1991; Campbell and Shiozawa, 1992; Fredlund and Xing, 1994; Fayer and Simmons, 1995; Rossi and Nimmo, 1994; Webb, 2000; Lu et al., 2008). Groenevelt and Grant (2004) theoretically derived the value of h_0 as $10^{4.9}$ m using the Schofield (1935) equation, which corresponds to 52 % relative humidity at 20 °C (or 1 % relative humidity at 105 °C). Schneider and Goss (2012) presented a different value for h_0 , $10^{4.8}$ m, which represents the average value for a relative humidity between 30 % and 70 % at 20 °C (equivalent to a relative humidity between 0.6 % and 1.8 % at 105 $^{\circ}\text{C}$ as estimated via the Kelvin equation). They found that an h_0 value of $10^{4.8}$ m agrees better with the literature data than that of 10⁵ m. However, Arthur et al. (2013) pointed out that this outperformance could be attributed to the fact that the lowest suction value in the dataset used by Schneider and Goss (2012) ranged from 10^{4.0} to 10^{4.4} m.

The PDI model incorporates h_0 in both the capillary and adsorption water components (Eqs. [C2] and [C4]), ensuring that they converge to zero at h_0 . Consequently, the value of h_0 impacts the PDI model fitted results, and thus the θ^* hc value estimated from model parameters. Fig. 2 displays the PDI model fitted θ values with $h_0=10^5$ m, $h_0=10^{4.9}$ m and $h_0=10^{4.8}$ m versus the measured values for soils in the calibration dataset. Surprisingly, for various h_0 values, the fitted results are similar with all points distributed closely along the 1:1 line, the slopes of the regression lines are close to unity, and the intercepts are zero. For $h_0=10^5$ m, the average root mean squared error (RMSE), average mean error (ME) and average relative error (RE) values between the fitted results with PDI model and the measured θ values were 0.009, 0.007 and 9.5 %,

Table 1 Soil ID, texture, particle size distribution (PSD), quartz content, porosity (ϕ), organic carbon content, and sources of soils (Soils 1–25) data used for model calibration in this study. The star symbol identifies ϕ values calculated from actual bulk density values with an assumed particle density value of 2.65 g cm⁻³.

Soil ID	Soil name or texture	Particle size distribution			Quartz content	ф			Sources
		2-0.05 mm	0.05–0.002 mm	<0.002 mm			log ₁₀ (h) range	λ range	
		g g ⁻¹			g g ⁻¹	$\mathrm{m^3~m^{-3}}$	m	${\rm W} {\rm \ m}^{-1} {\rm \ K}^{-1}$	
1	Quincy sand	0.95	0.03	0.02	0.63	0.43	0.2 - 5.0	0.2 - 1.4	McInnes (1981)
2	Ritzville silt loam	0.30	0.64	0.06	0.42	0.53	0 - 4.2	0.2 - 1.0	McInnes (1981)
3	Walla Walla silt loam	0.30	0.61	0.09	0.42	0.53	0.3 - 5.0	0.2 - 0.9	McInnes (1981)
4	Palouse silt loam	0.20	0.68	0.12	0.38	0.53	0.5 - 5.0	0.2 - 0.9	McInnes (1981)
5	Naff silt loam	0.20	0.57	0.23	0.45	0.53	1.0 - 4.6	0.2 - 1.0	McInnes (1981)
6	L-soil	0.91	0.07	0.02	_	0.45	-0.5 - 3.8	0.2 - 1.0	Cass et al. (1981)
7	Accusand 12/20	1	0	0	1	0.32*	-1.70.1	0.3 - 2.9	Deepagoda et al. (2016)
8	Accusand 20/30	1	0	0	1	0.33*	-2.60.5	0.3 - 2.9	Deepagoda et al. (2016)
9	Accusand 30/40	1	0	0	1	0.34*	-3.0 - 0.2	0.3 - 2.9	Deepagoda et al. (2016)
10	Accusand 40/50	1	0	0	1	0.35*	-1.20.3	0.3 - 2.9	Deepagoda et al. (2016)
11	Accusand 50/70	1	0	0	1	0.34*	-1.4 - 0	0.4 - 3.3	Deepagoda et al. (2016)
12	Soil A	_	_	_	0.69	0.38*	-1.2 - 0.8	0.6 - 2.7	Wu et al. (2015)
13	Soil B	_	_	_	0.77	0.36*	-1.1 - 0.7	0.4 - 1.7	Wu et al. (2015)
14	Soil C	_	_	_	0.78	0.32*	-1.1 - 0.6	0.4 - 2.7	Wu et al. (2015)
15	Liuzhou lateritic clay	0.12	0.41	0.48	0.44	0.60	-1.0 - 3.2	0.2 - 1.0	Xu et al. (2019)
16	Guilin lateritic clay	0.14	0.32	0.54	0.12	0.60	-1.0 - 3.8	0.3 - 1.2	Xu et al. (2019)
17	sand	1	0	0	_	0.43*	-2.0 - 2.2	0.3 - 2.5	Fu et al. (2021b)
18	silt loam	0.21	0.67	0.12	_	0.60*	-2.0 - 2.2	0.2 - 1.1	Fu et al. (2021b)
19	clay loam	0.24	0.49	0.27	_	0.55*	-2.0 - 2.2	0.4 - 1.2	Fu et al. (2021b)
20	loam	0.43	0.37	0.20	_	0.60	0.5 - 2.2	0.2 - 1.1	Sepaskhah & Boersma (1979)
21	silty clay loam	0.09	0.64	0.27	_	0.60	0.5 - 2.2	0.2 - 1.0	Sepaskhah & Boersma (1979)
22	clay loam	0.32	0.38	0.30	_	0.51*	0.4 - 5.0	0.2 - 1.4	Lu et al. (2007)
23	sand	0.92	0.07	0.01	_	0.40*	-0.4 - 5.0	0.2 - 2.1	Lu et al. (2007)
24	sandy loam	0.67	0.21	0.12	_	0.48*	-1.3 - 4.4	0.2 - 1.7	Lu et al. (2008)
25	loam	0.40	0.49	0.11	_	0.51*	-1.0 - 5.0	0.2 - 1.6	Lu et al. (2008)

Table 2 Soil ID, texture, particle size distribution (PSD), quartz content, porosity (ϕ), and sources of soils (Soils 26–31) data used for model validation in this study. The star symbol identifies ϕ values calculated from actual bulk density values with an assumed particle density value of 2.65 g cm⁻³.

Soil ID	Soil name or texture	Particle size distribution			Quartz content	ф			Sources
		2–0.05 mm	0.05-0.002 mm	<0.002 mm			log ₁₀ (h) range	λ range	
		g g ⁻¹	g g ⁻¹	g g ⁻¹	g g ⁻¹	$\mathrm{m}^3~\mathrm{m}^{-3}$	m	${\rm W} {\rm \ m}^{-1} {\rm \ K}^{-1}$	
26	sand	0.93	0.01	0.06	_	0.40*	-2.0 - 4.0	0.3 - 2.1	Lu et al. (2008
27	silt loam	0.27	0.51	0.22	_	0.50*	-1.0 - 5.0	0.2 - 1.4	Lu et al. (2008
28	silt loam	0.11	0.70	0.19	_	0.51*	-0.3 - 5.0	0.3 - 1.6	Lu et al. (2008
29	silty clay loam	0.19	0.54	0.27	_	0.51*	-1.0 - 5.0	0.2 - 1.4	Lu et al. (2008
30	silty clay loam	0.08	0.60	0.32	_	0.51*	-0.3 - 5.0	0.2 - 1.3	Lu et al. (2008
31	silt loam	0.02	0.73	0.25	_	0.55*	-1.0 - 5.0	0.2 - 1.2	Lu et al. (2008

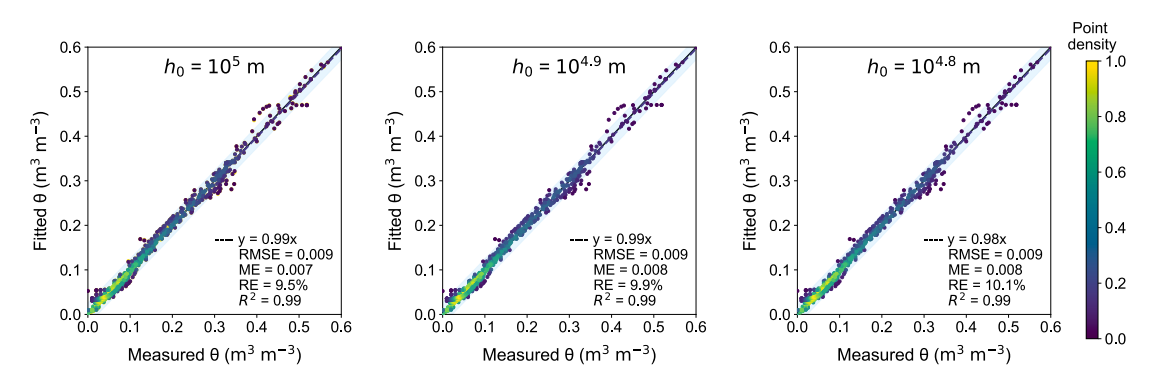


Fig. 2. Comparison of fitted θ values with the PDI model using three h_0 values versus measured θ values for Soils 1–25 in the calibration dataset. The solid lines are the 1:1 lines, the dashed lines represent the regression lines and the blue regions indicate 95% prediction intervals. (For interpretation of the references to colour in this figure legend, the reader is referred to the web version of this article.)

respectively, which were equal to or lower compared than the cases with $h_0 = 10^{4.9}$ m and $10^{4.8}$ m. Thus, we set h_0 as 10^5 m hereafter, although this is different from the original PDI model value (i.e., $10^{4.8}$ m) suggested by Peters (2013) following Schneider and Goss (2012). Our results are also consistent with Arthur et al. (2013), who determined the

average h_0 value should be kept at $10^{4.9}$ m or $10^{5.0}$ m using a larger dataset including data from Schneider and Goss (2012). We must emphasize here that using a fixed h_0 does have merit: Campbell et al. (1993) found a strong correlation between water content at 0.1 m and clay content using $h_0 = 10^{5.0}$ m; Schneider and Goss (2012) established a

nonlinear relationship between the slope of the dry part of a SWRC and clay content by fixing h_0 at $10^{4.8}$ m. However, recent studies indicate that h_0 is not a constant quantity, but strongly depends on the soil mineral composition and can vary between $10^{4.7}$ and $10^{5.1}$ m (Lu and Khorshidi, 2015) and be $10^{5.1}$ m in quartz minerals (Zhang et al., 2017).

4.2. Comparison of vG and PDI model parameters

Fig. 3 presents a comparison of model parameters, fitted under three distinct scenarios: (1) employing the vG model with limited SWRC data ranging from 0 to 150 m; (2) utilizing the vG model with a full range of SWRC data from 0 to 10⁵ m; and (3) applying the PDI model with a full range of SWRC data. These scenarios are evaluated across 25 different soils included in our calibration dataset. In all cases, the fitted θ_s values are consistently similar, with all data points closely distributed along the 1:1 line. Interestingly, the α and n values in case 1 are closer to those in case 3 than those in case 2. This suggests two important conclusions: first, the discrepancy primarily stems from the contrasting abilities of the vG and PDI models to fit SWRC data, rather than on the range of SWRC data; second, adopting only the wet part (i.e., 0 to 150 m), rather than the full SWRC data, for fitting the vG model can potentially enhance the fitting accuracy in comparison to the PDI model results. This also justifies previous studies which used h = 150 m as the boundary between wet and dry ends when developing their models (e.g., Fayer and Simmons, 1995; Lu et al., 2008; Jensen et al., 2015). Additionally, the comparison of results for 1/n tends to be more dispersed for low n values, which are characteristic of fine-textured soils. Coarsetextured soils generally have low water content values at h = 150 m (i.e., permanent wilting point), thus fitting the vG or PDI models to either full range or limited range SWRC data does not significantly influence the fitted parameters.

A major discrepancy between vG and PDI model fitted parameters occurs with respect to θ_r : for several soils, vG model yields $\theta_r=0$, whereas PDI model fitted θ_r values can be as large as 0.254 m3/m $^{-3}(-|-)$ (Fig. 3). Such differences can be attributed to divergent interpretations of θ_r in the two models. In the vG model, θ_r is regarded purely as an adjustable parameter, representing the point at which the slope of the

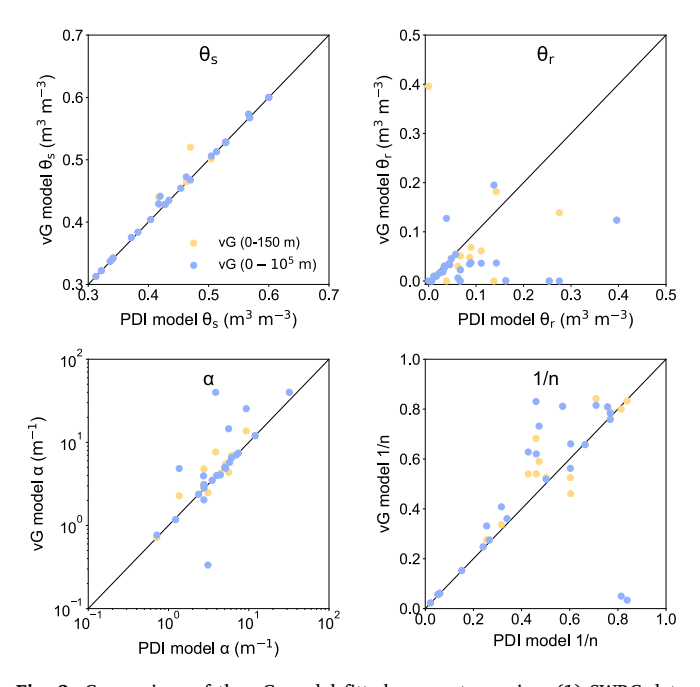


Fig. 3. Comparison of the vG model fitted parameters using: (1) SWRC data from 0 to 150 m; (2) SWRC from 0 to 10^5 m versus PDI model (using SWRC data from 0 to 10^5 m) for Soils 1–25 in the calibration dataset. The solid lines are the 1:1 lines.

SWRC approaches zero (i.e., $d\theta/dh=0$). Consequently, when fitting the vG model to a full range of SWRC data, which include measurements of the lowest θ values near zero, it is unsurprising that the vG model obtains $\theta_r=0$. As a result, many pedo-transfer functions based on the vG model assume $\theta_r=0$ (Wösten et al., 1999; Zacharias and Wessolek, 2007; Weynants et al., 2009). In contrast, Iden and Durner (2014) proposed θ_r as the weighting factor for adsorption saturation (S_{ads} in Eq. [C4]), thus identical to the adsorption capacity or maximum water content ascribed to adsorption forces (θ max ads). It can be theoretically derived as (Revil and Lu, 2013; Lu, 2016):

$$\theta_{r} = \theta_{ads}^{max} = \frac{(1-\varphi)\rho_{s}}{\rho_{w}} \frac{CEC}{\overline{\xi}} \tag{20} \label{eq:20}$$

where ρ_s is particle density (approximately 2.65 Mg/m⁻³(-|-) for many soils), $\rho_{\rm w}$ is density of water (1 Mg/m⁻³(-|-)), CEC is cation exchange capacity (meq g^{-1}) and ξ is a sorption parameter (1.6meq g^{-1} for Kaolinite and Illite, 2.8meq g⁻¹ for Smectite and Vermiculite). As CEC is heavily influenced by clay content, it is expected that the fitted θ_r values in the PDI model display a strong correlation with clay content, as depicted in Fig. 4. It is noteworthy that Soils 15-16 are excluded from the regression between θ_r and clay content as they are typical dualporosity soils which cannot be well described by the unimodal vG model used in the capillary component of PDI model (i.e., Eq. [C3)). Peters et al. (2013) suggested that the saturation function, denoted as $\Gamma(h)$, can be either unimodal or multimodal models (Durner, 1994; Weber et al., 2017). Thus, it is interesting to explore the application of multimodal SWRC models, for instance, those proposed by Durner (1994), in conjunction with multi-region $\lambda(\theta)$ models (e.g., Eqs. [8]-[11] in Deepagoda et al. (2016)) for heterogeneous soils characterized by a multi-pore size distribution. However, this is outside the scope of our study, thus will not be further discussed here.

4.3. Determination of parameters

After setting h_0 to $10^{5.0}$ m, we begin to fit the GD and PDI models to the measured $\lambda(\theta)$ and SWRC data for the 25 soils in the calibration dataset. Subsequently, the model parameters, along with θ^* hc, are determined. Variations in 1/n and θ^* hc as a function of θ_c are depicted in Fig. 5. As expected, both 1/n and θ^* hc increased monotonously with increasing θ_c . The trend is reasonable as fine-textured soils possess larger surface area and more meso- or micro- pores than coarse-textured soils. Consequently, they exhibit larger θ_c values (i.e., more water needed to form the water bridges), smaller n values (i.e., wider pore size

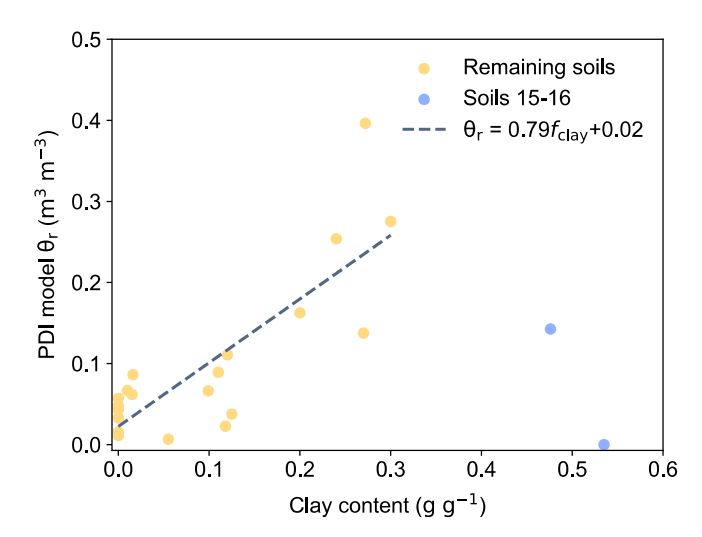


Fig. 4. PDI model fitted θ_r as a function of clay content for Soils 1–25 in the calibration dataset. The dashed line is the regression line for Soils 1–25 after excluding Soils 15 and 16.

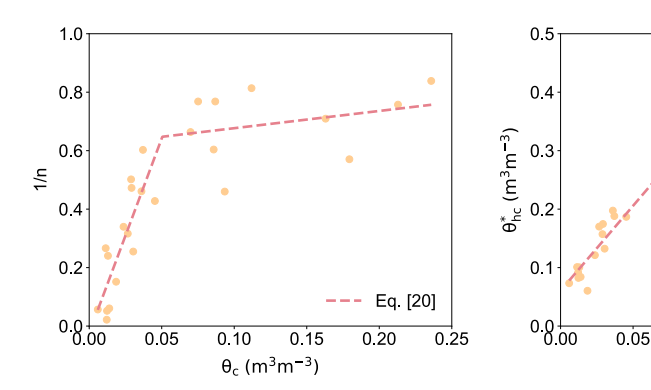


Fig. 5. The inverse of the pore size distribution parameter (1/n) and the hydraulic continuity water content (θ_{hc}) versus θ_c for Soils 1–25 in the calibration dataset. The dashed lines represent the fitted relationships in the GD-PDI approaches (Eqs. [21] and [22]).

distribution) and larger θ_{hc} values (i.e., stronger water holding ability against the force of gravity and viscous dissipation). Additionally, both 1/n and θ^* hc increase significantly at relatively low θ_c values followed by less steep slopes toward the high θ_c regime. Fig. 5 illustrates this transition, where the inflection points for the change in slope occur at 0.05 m³ m⁻³ for 1/n and 0.09 m³ m⁻³ for θ^* hc in relation to θ_c . To model this behavior, we have employed piecewise linear functions with two segments, developed using the SciPy library in Python. These functions exhibit high goodness-of-fit values (R² of 0.83 and 0.96) and effectively capture the observed 1/n vs θ_c and θ^* hc vs θ_c relationships as follows:

$$1/n = 13.306\theta_c - 0.017 \quad \theta_c < 0.050$$
 (21a)

$$1/n = 0.590\theta_{c} + 0.618 \quad \theta_{c} \ge 0.050 \tag{21b}$$

$$\theta_{hc}^* = 2.902\theta_c + 0.059 \quad \theta_c < 0.094$$
 (22a)

$$\theta_{bc}^* = 0.580\theta_c + 0.278 \quad \theta_c > 0.094$$
 (22b)

The parameters in Eq. [16] are determined based on fitting, leading to the following function ($R^2 = 0.87$):

$$\theta_{\rm s} = 0.034 + 0.007 f_{\rm sand} + 0.889 \phi \tag{23}$$

The coefficient of ϕ is less than one, which aligns with the expectation that θ_s should not exceed ϕ . Furthermore, it is evident that the sand content exerts a negligible effect on θ_s . This agrees with findings from earlier pedo-transfer functions (e.g., Zacharias and Wessolek, 2007; Weynants et al., 2009), though these functions focused on estimating θ_s of the vG model. The rationale behind this correlation is supported by the data presented in Fig. 3, which illustrate that the fitted θ_s values from both the PDI and vG models are similar.

Next, based on 22 soils in the calibration dataset (Soils 12–14 were excluded because of unavailable texture information), we established the following pedo-transfer function to estimate parameter α (R² = 0.86),

$$ln(\alpha) = 8.619 - 9.279 f_{clav} - 14.627 \phi - 1.951 ln(\lambda_{sat}) + 20.348 \theta_c \tag{24} \label{eq:24}$$

The predictors in Eq. [24] include clay content, porosity, λ_{sat} and θ_c . Using a combination of differential effective medium theory and the geometric mean method, Fu et al. (2023d) found that λ_{sat} is predominantly influenced by particle size distribution, particle shape and porosity, and suggested that λ_{sat} can be calculated from sand content and porosity. The parameter θ_c of the GD model, as reported in prior studies (Sadeghi et al., 2018; Fu et al. 2023c), has a demonstrable connection to porosity and soil texture. As a consequence, Eq. [24] bears a resemblance to the SCBD (Sand, Clay, and Bulk Density) based pedo-transfer functions developed earlier (e.g., Rosetta, Schaap et al., 2001; Zhang and Schaap, 2017).

4.4. Evaluation of the GD-PDI approach

0 10

 $\theta_c (m^3 m^{-3})$

0.15

In the preceding section, we developed an approach to determine the PDI model parameters: the pore size distribution parameter n was estimated from the critical water content θ_c , using Eq. [21]; saturated water content θ_s was calculated from sand content and porosity, as per Eq. [23]; α was determined from clay content, porosity, λ_{sat} and GD model parameters t_s and θ_c , according to Eq. [24]; and residual water content θ_r was estimated with Eq. [22] once the remaining parameters were known. Therefore, this new approach is hereafter, denoted as the "GD-PDI" approach.

Eq. [21]

0.25

0.20

Fig. 6 illustrates the estimated SWRCs obtained from the GD-PDI and GD-vG approaches, in comparison to the measured SWRC values for Soils 26–31 in the validation dataset. Within the wet range (h ranging from 0 to 150 m), both approaches generally exhibit patterns that align with the measured curves. However, their performance differs in the dry range (i.e., h > 150 m): the vG model estimated SWRCs tend to be flatter and overestimate the observations. This is because the vG model predicts θ values that approach θ_r at high h values, while the dry end of the SWRC usually decreases linearly toward 0 on a semi-log scale (Campbell and Shiozawa, 1992). In contrast, the PDI model incorporates a smoothed piecewise linear function to ensure a gradual linear decrease in θ for $h \gg 1/\alpha$ (Iden and Durner, 2014). Thus, the GD-PDI approach proposed in this study, known as the PDI model-based approach, accurately captures both the SWRC sigmoidal shape in the wet range and the linear trend at the dry end.

Fig. 7 presents estimated θ as a function of h with the GD-PDI and GD-vG approaches compared to the measured θ data. Consistent with the findings in Fig. 6, the GD-PDI approach exhibits superior performance over the GD-vG approach in several aspects. The GD-PDI approach provides a lower average RMSE (0.022 vs 0.028 m³ m³), lower average ME (0.017 vs 0.023 m³ m³), lower average RE (11.4 % vs 22.5 %), higher slope of regression line (1.00 vs 0.93) and higher R² (0.98 vs 0.97). Among all the metrics, the most significant difference between the two approaches is observed in the RE, which proves to be highly sensitive to low θ values. The RE values for the GD-PDI approach range from 7.8 % to 17.4 %, while the GD-vG approach yields REs ranging from 13.6 % to 38.4 % (Table 3).

We also compared results between the estimated and measured SWRCs for an h range exceeding 150 m. The findings, as depicted in Fig. 8, clearly demonstrate the consistent accuracy of the GD-PDI approach, with datapoints from saturation to dry closely distributed along the 1:1 line. In contrast, the GD-vG approach exhibited a worse performance in the dry range with average RMSE of 0.027 m³ m³, average ME of 0.022 m³ m³, average RE of 67 % and R² of 0.64 in comparison to the GD-PDI approach with average RMSE of 0.007 m³ m³, average ME of 0.006 m³ m³, average RE of 15.9 % and R² of 0.97 for the same validation dataset. For θ values for a h range larger than 150 m H₂O, the RE values for six soils by the GD-PDI approach ranges

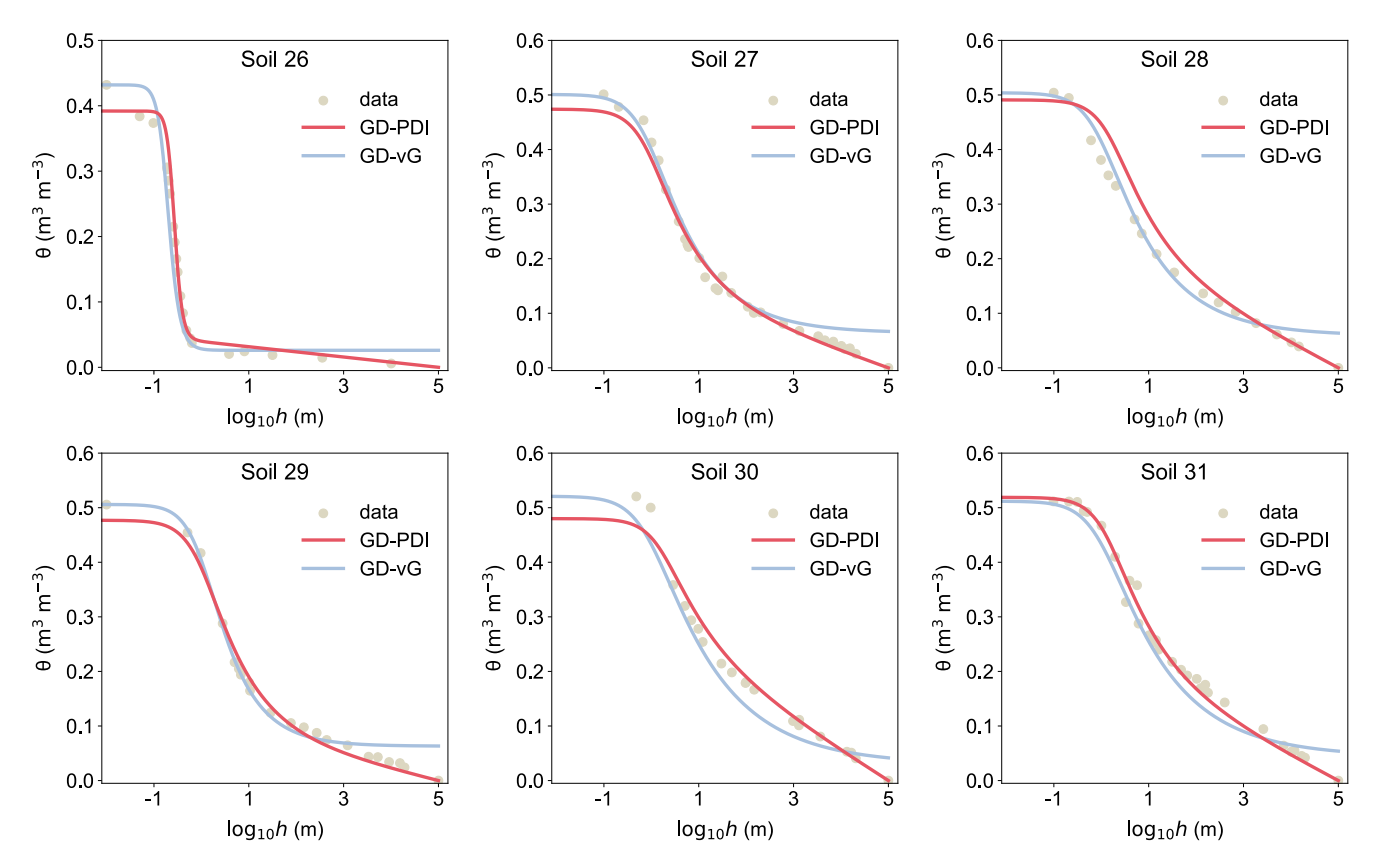


Fig. 6. Measured and estimated soil water retention curves (SWRC) with the GD-PDI and GD-vG approaches for Soils 26-31.

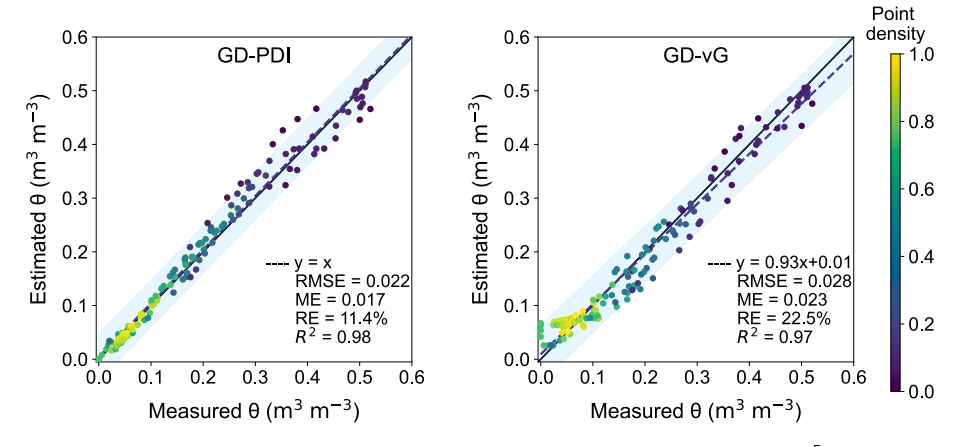


Fig. 7. θ values estimated by the GD-PDI and GD-vG approaches versus measured θ values at suction values from 0 to 10^5 m for Soils 26–31 in this study. The solid lines are the 1:1 lines, the dashed lines represent the regression lines and the blue regions indicate 95 % prediction intervals. (For interpretation of the references to colour in this figure legend, the reader is referred to the web version of this article.)

from 3 % to 31 %, whereas the GD-vG approach yields REs ranging from 18 % to 208 % (Table 4). Moreover, the majority of data points using the GD-vG approach exhibited a deviation from the 1:1 line, as evidenced by a regression line with a slope of merely 0.38. These results, again, demonstrate the superior performance of the GD-PDI approach over the GD-vG approach, particularly in the dry range, which is crucially important for simulating water transport and biochemical processes in soils.

4.5. Further discussion

Independent validation indicates that the GD-PDI approach performs well over the entire range of saturation. However, several important facts regarding this approach must be addressed here.

First, the GD-PDI approach is primarily developed using mineral soils collected from the field and repacked in the lab, which differ significantly from peat soils with high organic matter content or undisturbed soils with strong structure. It is well known that mineral soils typically have lower organic matter content, whereas peat soils are rich in organic matter, which significantly affects their thermal properties. For example, Zhao et al. (2019) found that λ values as a function of θ for peat soils are less than 20 % of those for sandy soils. More importantly, the $\lambda(\theta)$ curves for peat soils exhibit a concave downward shape, lacking the "flat tail" characteristic of most fine-textured soils. Similarly, Schjønning (2021) reported that undisturbed soils have a much wider range of $\lambda_{\rm sat}$ and $\lambda_{\rm dry}$ than those typically found in the literature. These differences will inevitably affect the fitted $\theta_{\rm c}$ and $t_{\rm s}$ values, thereby challenging the validity of the established relationships. Additionally, the well-

Table 3
The root mean square error (RMSE), mean error (ME), relative error (RE) and coefficient of determination (R²) between measured and estimated water content values from the GD-PDI and GD-vG approaches for Soils 26–31.

Soils ID	Soil name or texture	GD-PDI				GD-vG			
		RMSE	ME	RE	R ²	RMSE	ME	RE	R ²
		$m^3 m^{-3}$	m ³ m ⁻³	%		$m^3 m^{-3}$	m ³ m ⁻³	%	
21	sand	0.023	0.018	17.4	0.98	0.039	0.031	38.4	0.94
22	silt loam	0.016	0.012	9.4	0.99	0.024	0.020	27.8	0.99
23	silty clay loam	0.039	0.028	11.3	0.97	0.024	0.018	13.6	0.98
24	silt loam	0.016	0.014	14.8	0.99	0.021	0.015	26.2	0.98
25	silty clay loam	0.023	0.017	7.8	0.98	0.032	0.028	14.9	0.98
26	silt loam	0.015	0.011	7.8	0.99	0.029	0.025	14.1	0.98
Average		0.022	0.016	11.4	0.98	0.028	0.023	22.5	0.97

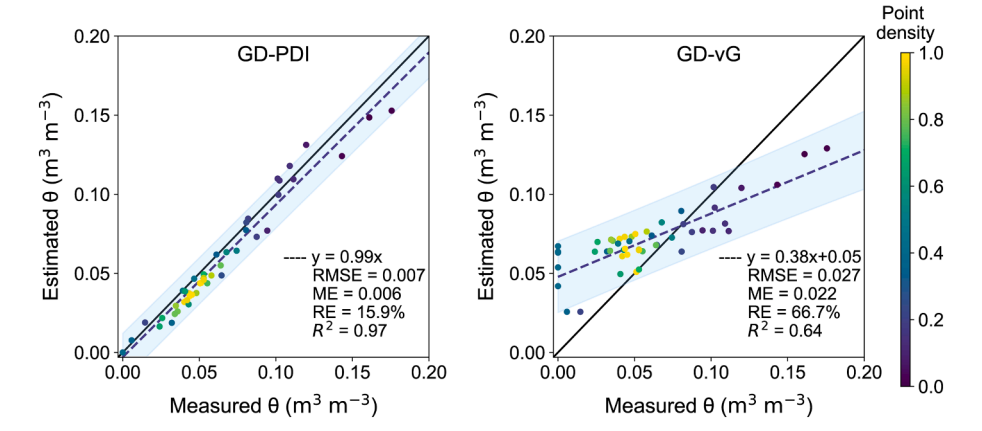


Fig. 8. Estimated θ values by the GD-PDI and GD-vG approaches versus measured θ values at suction values higher than 150 m for Soils 26–31 in this study. The solid lines are the 1:1 lines, the dashed lines represent the regression lines and the blue regions indicate 95 % prediction intervals. (For interpretation of the references to colour in this figure legend, the reader is referred to the web version of this article.)

Table 4

The root mean square error (RMSE), mean error (ME), relative error (RE) and coefficient of determination (R²) between measured and estimated water content values at suction values higher than 150 m from the GD-PDI and GD-vG approaches for Soils 26–31.

Soils ID	Soil name or texture	GD-PDI				GD-vG			
		RMSE	ME	RE	R ²	RMSE	ME	RE	R ²
		$m^3 m^{-3}$	m ³ m ⁻³	%		$m^3 m^{-3}$	m ³ m ⁻³	%	
21	sand	0.003	0.003	30.6	1.00	0.016	0.015	207.9	1.00
22	silt loam	0.007	0.006	14.3	0.98	0.033	0.028	62.4	0.85
23	silty clay loam	0.005	0.003	3.4	1.00	0.029	0.022	28.6	0.90
24	silt loam	0.011	0.010	25.5	0.98	0.031	0.025	59.1	0.83
25	silty clay loam	0.005	0.004	6.6	0.99	0.024	0.019	17.8	0.93
26	silt loam	0.013	0.011	15.2	1.00	0.029	0.024	24.2	0.95
Average		0.007	0.006	15.9	0.97	0.027	0.022	66.7	0.64

developed structure of undisturbed soils often leads to bimodal or trimodal pore size distributions, which means that the unimodal vG model used for capillary water in this study may not apply to them. This will influence the fitted PDI model parameters, further affecting the validity of the established relationships. Therefore, it is crucial to further investigate and develop the relationships between $\lambda(\theta)$ and SWRC using a broader range of soils, including organic and structured soils, to improve the model's applicability and robustness.

Second, the approach was calibrated and validated using a limited dataset—25 soils for calibration and 6 for validation. This limitation stems from the difficulty of obtaining concurrent measurements of both $\lambda(\theta)$ and SWRC. Previous studies often relied on a custom-built apparatus (e.g., Smits et al., 2013; Lu et al., 2019) to measure these properties simultaneously. However, these devices are challenging to build and prone to variability, and have thus not been widely adopted, which has led to a scarcity of soils in the literature with both $\lambda(\theta)$ and SWRC data. Recently, the development of commercial equipment, such as the

VARIOS/HYPROP connector (METER, Pullman, WA), enables the simultaneous measurement of thermal and hydraulic properties in a more reliable and accessible manner. This advancement is expected to increase the availability of $\lambda(\theta)$ and SWRC data for soil samples, providing an excellent opportunity to derive more robust and general relationships between $\lambda(\theta)$ and SWRC using machine learning algorithms, which are powerful but require large datasets to function effectively.

Finally, the GD-PDI approach is parametric, relying on four equations (Eqs. [21]-[24]) to estimate the PDI model parameters. This approach is designed to minimize the sum of squared errors (SSE) between fitted and estimated parameters. However, errors in the estimation of each parameter inevitably propagate into the final estimation of soil θ , which can explain the variability observed in the GD-PDI model results shown in Figs. 6-8. We choose to estimate each parameter independently rather than develop all equations simultaneously because the latter will introduce more unknown coefficients that need to be

fitted. Given the small dataset used in this study, fitting all parameters together will likely lead to overfitting issues. As mentioned earlier, once more comprehensive $\lambda(\theta)$ and SWRC data become available, neural networks can be employed to develop a novel method to estimate the SWRC from $\lambda(\theta)$ measurements. In this approach, the objective function minimizes the SSE between fitted and estimated θ without relying on pre-assumed relationships (e.g., Eqs. [14]–[17]), potentially leading to more accurate predictions and a more robust overall performance (Rudiyanto et al., 2021).

5. Summary and conclusions

Based on the inherent connection between soil water retention and $\lambda(\theta)$ curves, Fu et al. (2023a) proposed a method to estimate the vG model parameters from measured $\lambda(\theta)$ data. However, the method inherits the constraints of the vG model, primarily its ineffectiveness in the dry segment of the SWRC, notably in the adsorption region. In this study, we formed correlations between GD model parameters and SWRCs modeled by the PDI model, which was selected because of its ability to describe a SWRC over the complete moisture range and distinguish the capillary and adsorption water components.

We first proposed linearization procedures to determine the hydraulic continuity water content (θ^* hc), below which hydraulic continuity for capillary flow is interrupted, based on the capillary component of the PDI model. Two piecewise linear functions were then formulated to relate θ^* hc and the pore size distribution parameter n with the GD model parameter θ_c . In conjunction with the pedo-transfer functions to estimate the vG model parameters θ_s and α from sand content, clay content, porosity and GD parameters, a novel approach was developed to estimate the PDI model parameters from $\lambda(\theta)$ measurements. The GD-PDI approach was tested using six independent soils and GD-PDI results

were compared to results from the GD-vG approach. The GD-PDI approach outperformed the GD-vG approach, particularly in the dry end of the SWRC, i.e., when h>150 m. The superior performance observed in the dry range has particular importance for simulations of the intricate dynamics of water transport and biochemical processes in arid soils. We also acknowledge the need for user-friendly tools to simplify the application of the GD-PDI approach. To this end, an Excel file (.xlsm) is provided as Supplemental Material in Appendix D, which automates the calculation of PDI model parameters and the plotting of the SWRC using the GD-PDI approach.

CRediT authorship contribution statement

Yongwei Fu: Writing – original draft, Funding acquisition, Formal analysis, Conceptualization. Robert Horton: Writing – review & editing, Supervision, Funding acquisition, Conceptualization. Joshua Heitman:

Declaration of competing interest

The authors declare that they have no known competing financial interests or personal relationships that could have appeared to influence the work reported in this paper.

Acknowledgements

This research was supported by the National Natural Science Foundation of China (Grant Number: 42407414), US National Science Foundation (Grant Number: 2037504) and USDA-NIFA Multi-State Projects 4188 and 5188.

Appendix A

The Ghanbarian and Daigle (GD) model

Using a combination of percolation theory and an effective-medium approximation (GD), Ghanbarian and Daigle (2016) presented a model to describe the $\lambda(\theta)$ curve for unsaturated soils. Sadeghi et al. (2018) derived its explicit form as follows:

$$\lambda = \left[a_1 + a_2 \theta + sgn(t_s) a_2 \sqrt{a_3 + 2a_1 a_2^{-1} \theta + \theta^2} \right]^{t_s}$$
(A1)

where t_s is a scaling exponent. Theoretically, $t_s > 0$, and thus, the sign function (i.e., sgn(x > 0) = 1, sgn(x < 0) = -1) can be eliminated. The coefficients are given by:

$$a_1 = \frac{-\theta_c \lambda_{sat}^{1/t_s} + (\theta_s - \theta_c) \lambda_{dry}^{1/t_s}}{2(\theta_s - \theta_c)}$$
(A2)

$$a_{2} = \frac{\lambda_{sat}^{1/t_{s}} - \lambda_{dry}^{1/t_{s}}}{2(\theta_{s} - \theta_{c})} \tag{A3}$$

$$a_{3} = \frac{\left[\theta_{c}\lambda_{sat}^{1/t_{s}} - (\theta_{s} - \theta_{c})\lambda_{dry}^{1/t_{s}}\right]^{2} + 4\theta_{c}(\theta_{s} - \theta_{c})\lambda_{sat}^{1/t_{s}}\lambda_{dry}^{1/t_{s}}}{\left(\lambda_{sat}^{1/t_{s}} - \lambda_{dry}^{1/t_{s}}\right)^{2}}$$

$$(A4)$$

where θ_c is the critical water content at which water first forms a continuous path through the medium (i.e., 'water bridges' between solid particles).

Appendix B

Hydraulic continuity water content estimated from the van Genuchten model. The first and second derivatives of Eq. [1] are computed as

$$\frac{d\theta}{dh} = (\theta_{s} - \theta_{r})(-n+1)\alpha^{n}h^{n-1}[1 + (\alpha \ h)^{n}]^{(-2+1/n)}$$
(B1)

$$\frac{d^{2}\theta}{dh^{2}} = (\theta_{s} - \theta_{r})(n-1)\alpha^{n}h^{n-2}[1 + (\alpha \ h)^{n}]^{(-3+1/n)}\{1 + n[(\alpha \ h)^{n} - 1]\}$$
(B2)

By setting $\frac{d^2\theta}{dh^2} = 0$, we determine the suction at the inflection point (h_i) as

$$h_{\rm i} = \frac{1}{\alpha} \left(1 - \frac{1}{n} \right)^{1/n} \tag{B3}$$

Substituting Eq. [B3] into Eq. [1] gives the water content at the inflection point $(\boldsymbol{\theta}_i)$ as

$$\theta_{\rm i} = (\theta_{\rm s} - \theta_{\rm r}) \left(2 - \frac{1}{n}\right)^{-1 + 1/n} + \theta_{\rm r} \tag{B4}$$

The slope at the inflection point is thus obtained by substituting Eq. [A4] into Eq. [A1], which gives,

$$\left[\frac{d\theta}{dh}\right]_{h=h_i} = (\theta_s - \theta_r)\alpha(-n+1)\left(1 - \frac{1}{n}\right)^{(1-1/n)}\left(2 - \frac{1}{n}\right)^{(-2+1/n)} \tag{B5}$$

Eq. [B5] is similar to the "soil physical quality index (S)" proposed by Dexter (2004) but their expressions are different: the former is derived for θ vs h curve whereas S was defined based on SWRC plotted as θ vs $\ln(h)$.

Following the linearization method presented in Fig. 1a (Lehmann et al., 2008; Assouline and Or, 2014), the suction at which hydraulic continuity for capillary flow is interrupted (h_{hc}) is given by

$$h_{\rm hc} = \frac{1}{\alpha} \left(1 - \frac{1}{n} \right)^{1/n - 2}$$
 (B6)

Substituting Eq. [B6] into Eq. [1] leads to the following expression for hydraulic continuity water content (θ_{hc}):

$$\theta_{\rm hc} = (\theta_{\rm s} - \theta_{\rm r}) \left[1 + \left(\frac{n-1}{n} \right)^{1-2n} \right]^{\frac{1-n}{n}} + \theta_{\rm r} \tag{B7}$$

Appendix C

The Peters-Durner-Iden (PDI) retention model

For a fixed suction, the equilibrium water content can be divided into two components: capillary water and adsorbed water. The total water content in soil is thus described by the following superposition of a capillary term (θ_{cap}) and an adsorptive term (θ_{ads}) (Iden and Durner, 2014):

$$\theta = \theta_{\text{cap}} + \theta_{\text{ads}} = (\theta_{\text{s}} - \theta_{\text{r}})S_{\text{cap}} + \theta_{\text{r}}S_{\text{ads}} \tag{C1}$$

where S_{cap} and S_{ads} are relative saturation of capillary and adsorbed water, respectively; θ_s is saturated water content; and θ_r is residual water content and maximum adsorbed water content (also denoted as "adsorption capacity" in Lu (2016)).

To meet the physical requirement that the capillary term reaches zero at oven dryness, S_{cap} must be expressed as a scale function in terms of a water retention function $\Gamma(h)$,

$$S_{\text{cap}} = \frac{\Gamma(h) - \Gamma(h_0)}{1 - \Gamma(h_0)} \tag{C2}$$

where h_0 is the suction at oven dryness. $\Gamma(h)$ can be any unimodal, multimodal water retention models or their combinations (e.g., Brooks and Corey, 1964; van Genuchten, 1980; Kosugi, 1994). In this study, the four-parameter unimodal model introduced by van Genuchten (1980) will be used,

$$\Gamma(h) = \left[1 + (\alpha \ h)^n\right]^{(1/n-1)} \tag{C3}$$

where α is related to inverse of the air-entry suction (h_a) and n is pore size distribution parameter.

The relative saturation of adsorbed water S_{ads} is given by a smoothed piecewise linear function (Iden and Durner, 2014; Peters et al., 2021):

$$S_{\text{ads}} = \frac{\ln(h/h_0) - b\ln\left[1 + (h_a/h)^{1/b}\right]}{\ln(h_0/h_a)} \tag{C4}$$

where h_a reflects the suction where S_a shifts smoothly towards a value of unity and is set to α^{-1} (Peters, 2013). b is a smoothing parameter expressed as follows:

$$b = b_0 \left(1 + 2 \frac{1 - e^{-b_1}}{n^2} \right) \tag{C5}$$

$$b_0 = 0.1 \ln 10$$
 (C6)

$$b_1 = \left(\frac{\theta_{\rm r}}{\theta_{\rm r} - \theta_{\rm s}}\right)^2 \tag{C7}$$

Appendix D. Supplementary data

Supplementary data to this article can be found online at https://doi.org/10.1016/j.jhydrol.2024.132138.

Data availability

Data will be made available on request.

References

- Arthur, E., Tuller, M., Moldrup, P., Resurreccion, A.C., Meding, M.S., Kawamoto, K., Komatsu, T., Jonge, L.W., 2013. Soil specific surface area and non-singularity of soilwater retention at low saturations. Soil Sci. Soc. Am. J. 77, 43–53.
- Assouline, S., Or, D., 2014. The concept of field capacity revisited: Defining intrinsic static and dynamic criteria for soil internal drainage dynamics. Water Resour. Res. 50, 4787–4802
- Brooks, R.H., Corey, A.T., 1964. Hydraulic properties of porous media. Colorado State University, Fort Collins, Hydrology Paper, No. 3, March.
- Campbell, G.S., Shiozawa, S., 1992. Prediction of hydraulic properties of soils using particle size distribution and bulk density data, International workshop on indirect methods for estimating the hydraulic properties of unsaturated soils. University of California Press, Berkely
- Campbell, G.S., Jungbauer, J.D., Shiozawa, S., Hungerford, R.D., 1993. A one-parameter equation for water sorption isotherms of soils. Soil Sci. 156, 302–305.
- Carsel, R.F., Parrish, R.S., 1988. Developing joint probability distributions of soil water retention characteristics. Water Resour. Res. 24, 755–769.
- Cass, A.G., Campbell, G.S., Jones, T.L., 1981. Hydraulic and thermal properties of soil samples from the buried waste test facility. PNL-4015, Pacific Northwest Laboratory, Richland.
- Dai, Y., Xin, Q., Wei, N., Zhang, Y., Shangguan, W., Yuan, H., Zhang, S., Liu, S., Lu, X., 2019. A global high-resolution data set of soil hydraulic and thermal properties for land surface modeling. J. Adv. Model Earth Sy. 11, 2996–3023.
- Deepagoda, T.K.K.C., Smits, K., Ramirez, J., Moldrup, P., 2016. Characterization of thermal, hydraulic, and gas diffusion properties in variably saturated sand grades. Vadose Zone J. 15, 1–11.
- Durner, W., 1994. Hydraulic conductivity estimation for soils with heterogeneous pore structure. Water Resour. Res. 30, 211–223.
- Fayer, M.J., Hillel, D., 1986. Air encapsulation: I. Measurement in a field soil. Soil Sci. Soc. Am. J. 50, 568–572.
- Fayer, M.J., Simmons, C.S., 1995. Modified Soil Water Retention Functions for All Matric Suctions. Water Resour. Res. 31, 1233–1238.
- Fredlund, D.G., Xing, A., 1994. Equations for the soil-water characteristic curve. Can. Geotech. J. 31, 521-532.
- Fu, Y., Lu, S., Ren, T., Horton, R., Heitman, J.L., 2021a. Estimating soil water retention curves from soil thermal conductivity measurements. J. Hydrol. 127171.
- Fu, Y., Horton, R., Heitman, J., 2021b. Estimation of soil water retention curves from soil bulk electrical conductivity and water content measurements. Soil Tillage Res. 209, 104948
- Fu, Y., Liu, L., Lu, Y., Horton, R., Ren, T., Heitman, J., 2023a. Estimating soil water retention curves from thermal conductivity measurements: a percolation-based effective-medium approximation. J. Hydrol. 129898.
- Fu, Y., Ghanbarian, B., Horton, R., Heitman, J., 2023b. New insights into the correlation between soil thermal conductivity and water retention in unsaturated soils. Vadose Zone J. 23.
- Fu, Y., Ghanbarian, B., Horton, R., Heitman, J., 2023c. Robust calibration and evaluation of a percolation-based effective-medium approximation model for thermal conductivity of unsaturated soils. Geoderma 438, 116631.
- Fu, Y., Jones, S., Horton, R., Heitman, J., 2023d. Excluding quartz content from the estimation of saturated soil thermal conductivity: combined use of differential effective medium theory and geometric mean method. Agric. For. Meteorol. 342, 100743
- Ghanbarian, B., Daigle, H., 2016. Thermal conductivity in porous media: percolation-based effective-medium approximation. Water Resour. Res. 52, 295–314.
- Groenevelt, P.H., Grant, C.D., 2004. A new model for the soil-water retention curve that solves the problem of residual water contents. Eur. J. Soil Sci. 55, 479–485.
- Haverkamp, R., Leij, F.J., Fuentes, C., Sciortino, A., Ross, P.J., 2005. Soil water retention:
 I. Introduction of a shape index. Soil Sci. Soc. Am. J. 69, 1881–1890.
- He, H., Liu, L., Dyck, M., Si, B., Lv, J., 2021. Modelling dry soil thermal conductivity. Soil Tillage Res. 213, 105093.
- Iden, S.C., Durner, W., 2014. Comment on "Simple consistent models for water retention and hydraulic conductivity in the complete moisture range" by A. Peters. Water Resour. Res. 50, 7530–7534.
- Jensen, D.K., Tuller, M., de Jonge, L.W., Arthur, E., Moldrup, P., 2015. A New Two-Stage Approach to predicting the soil water characteristic from saturation to oven-dryness. J. Hydrol. 521, 498–507.

- Johansen, O., 1975. Thermal conductivity of soils. Ph.D. diss. Norwegian Univ. of Science and Technol., Trondheim (CRREL draft transl. 637, 1977).
- Khlosi, M., Cornelis, W.M., Gabriels, D., Sin, G., 2006. Simple modification to describe the soil water retention curve between saturation and oven dryness. Water Resour. Res. 42.
- Kosugi, K., 1994. Three-parameter lognormal distribution model for soil water retention. Water Resour. Res. 30, 891-901.
- Lehmann, P., Assouline, S., Or, D., 2008. Characteristic lengths affecting evaporative drying of porous media. Phys. Rev. E 77, 056309.
- Lu, N., 2016. Generalized soil water retention equation for adsorption and capillarity. J. Geotech. Geoenviron. 142, 04016051.
- Lu, N., Dong, Y., 2015. Closed-form equation for thermal conductivity of unsaturated soils at room temperature. J. Geotech. Geoenviron. 141, 04015016.
- Lu, N., Khorshidi, M., 2015. Mechanisms for soil-water retention and hysteresis at high suction range. J. Geotech. Geoenviron. 141, 04015032.
- Lu, S., Ren, T., Gong, Y., Horton, R., 2007. An improved model for predicting soil thermal conductivity from water content at room temperature. Soil Sci. Soc. Am. J. 71, 8–14.
- Lu, S., Ren, T., Gong, Y., Horton, R., 2008. Evaluation of three models that describe soil water retention curves from saturation to oven dryness. Soil Sci. Soc. Am. J. 72, 1542–1546.
- Lu, S., Lu, Y., Peng, W., Ju, Z., Ren, T., 2019. A generalized relationship between thermal conductivity and matric suction of soils. Geoderma 337, 491–497.
- Luo, Y., Ghezzehei, T.A., Yu, Z., Berli, M., 2020. Modeling near-surface water redistribution in a desert soil. Vadose Zone J. 19.
- McInnes, K.J., 1981. Thermal conductivities of soils from dryland wheat regions of Eastern Washington (Master dissertation). Washington State University, Pullman, WA.
- Peters, A., 2013. Simple consistent models for water retention and hydraulic conductivity in the complete moisture range. Water Resour. Res. 49, 6765–6780.
- Peters, A., Hohenbrink, T.L., Iden, S.C., Durner, W., 2021. A simple model to predict hydraulic conductivity in medium to dry soil from the water retention curve. Water Resour. Res. 57.
- Peters, A., Hohenbrink, T.L., Iden, S.C., Genuchten, M.Th. van, Durner, W., 2023.
 Prediction of the absolute hydraulic conductivity function from soil water retention data. Hydrol. Earth Syst. Sc. 27, 1565–1582.
- Revil, A., Lu, N., 2013. Unified water isotherms for clayey porous materials. Water Resour. Res. 49, 5685–5699.
- Ross, P.J., Williams, J., Bristow, K.L., 1991. Equation for extending water-retention curves to dryness. Soil Sci. Soc. Am. J. 55, 923–927.
- Rossi, C., Nimmo, J.R., 1994. Modeling of soil water retention from saturation to oven dryness. Water Resour. Res. 30, 701–708.
- Rudiyanto, Minasny, B., Chaney, N.W., Maggi, F., Giap, S.G.E., Shah, R.M., Fiantis, D., Setiawan, B.I., 2021. Pedotransfer functions for estimating soil hydraulic properties from saturation to dryness. Geoderma 403, 115194.
- Sadeghi, M., Ghanbarian, B., Horton, R., 2018. Derivation of an explicit form of the percolation-based effective-medium approximation for thermal conductivity of partially saturated soils. Water Resour. Res. 54, 1389–1399.
- Schaap, M.G., Leij, F.J., Genuchten, M.Th. van, 2001. rosetta: a computer program for estimating soil hydraulic parameters with hierarchical pedotransfer functions. J. Hydrol. 251, 163–176.
- Schjønning, P., 2021. Thermal conductivity of undisturbed soil Measurements and predictions. Geoderma 402, 115188.
- Schneider, M., Goss, K.-U., 2012. Prediction of the water sorption isotherm in air dry soils. Geoderma 170, 64–69.
- Schofield, R.K. 1935. The pF of the water in soil. Transactions of 3rd International Congress of Soil Science, Volume 2. Plenary Session Papers, pp. 37–48. Oxford.
- Sepaskhah, A.R., Boersma, L., 1979. Thermal conductivity of soils as a function of temperature and water content. Soil Sci. Soc. Am. J. 43, 439–444.
- Smits, K.M., Sakaki, T., Howington, S.E., Peters, J.F., Illangasekare, T.H., 2013. Temperature dependence of thermal properties of sands across a wide range of temperatures (30–70°C). Vadose Zone J. 12 (vzj2012), 0033.
- Tarnawski, V.R., Gori, F., 2002. Enhancement of the cubic cell soil thermal conductivity model. Int. J. Energ. Res. 26, 143–157.
- Tarnawski, V.R., Momose, T., Leong, W.H., 2015. Assessing the impact of quartz content on the prediction of soil thermal conductivity. Géotechnique 59, 331–338.
- van Genuchten, M.T., 1980. A closed-form equation for predicting the hydraulic conductivity of unsaturated soils. Soil Sci. Soc. Am. J. 44, 892–898.
- Van Looy, K., Bouma, J., Herbst, M., Koestel, J., Minasny, B., Mishra, U., Montzka, C., Nemes, A., Pachepsky, Y.A., Padarian, J., Schaap, M.G., Tóth, B., Verhoef, A., Vanderborght, J., Ploeg, M.J., Weihermüller, L., Zacharias, S., Zhang, Y., Vereecken, H., 2017. Pedotransfer functions in earth system science: challenges and perspectives. Rev. Geophys. 55, 1199–1256.

- Vereecken, H., Amelung, W., Bauke, S.L., Bogena, H., Brüggemann, N., Montzka, C., Vanderborght, J., Bechtold, M., Blöschl, G., Carminati, A., Javaux, M., Konings, A.G., Kusche, J., Neuweiler, I., Or, D., Steele-Dunne, S., Verhoef, A., Young, M., Zhang, Y., 2022. Soil hydrology in the earth system. Nat. Rev. Earth Environ. 1–15.
- Wang, Y., Zhou, J., Ma, R., Zhu, G., Zhang, Y., 2022. Development of a new pedotransfer function addressing limitations in soil hydraulic models and observations. Water Resour. Res. 58.
- Webb, S.W., 2000. A simple extension of two-phase characteristic curves to include the dry region. Water Resour. Res. 36, 1425–1430.
- Weber, T.K.D., Finkel, M., Gonçalves, M., Vereecken, H., Diamantopoulos, E., 2020. Pedotransfer function for the brunswick soil hydraulic property model and comparison to the van Genuchten-Mualem model. Water Resour. Res. 56.
- Weber, T.K.D., Iden, S.C., Durner, W., 2017. Unsaturated hydraulic properties of Sphagnum moss and peat reveal trimodal pore-size distributions. Water Resour. Res. 53, 415–434
- Weynants, M., Vereecken, H., Javaux, M., 2009. Revisiting Vereecken Pedotransfer functions: introducing a closed-form Hydraulic Model. Vadose Zone J. 8, 86–95.
- Wösten, J.H.M., Lilly, A., Nemes, A., Bas, C.L., 1999. Development and use of a database of hydraulic properties of European soils. Geoderma 90, 169–185.
- Wu, R., Tinjum, J.M., Likos, W.J., 2015. Coupled thermal conductivity dryout curve and soil-water characteristic curve in modeling of shallow horizontal geothermal ground loops. Geotechn. Geol. Eng. 33, 193–205.
- Xu, Y., Sun, D., Zeng, Z., Lv, H., 2019. Effect of temperature on thermal conductivity of lateritic clays over a wide temperature range. Int. J. Heat Mass Tran. 138, 562–570.

- Zacharias, S., Wessolek, G., 2007. Excluding organic matter content from pedotransfer predictors of soil water retention. Soil Sci. Soc. Am. J. 71, 43–50.
- Zhai, Q., Rahardjo, H., 2012. Determination of soil-water characteristic curve variables. Comput. Geotech. 42, 37–43.
- Zhang, Z.F., 2011. Soil Water retention and relative permeability for conditions from oven-dry to full saturation. Vadose Zone J. 10, 1299–1308.
- Zhang, C., Dong, Y., Liu, Z., 2017. Lowest matric potential in quartz: Metadynamics evidence. Geophys. Res. Lett. 44, 1706–1713.
- Zhang, Y., Schaap, M.G., 2017. Weighted recalibration of the Rosetta pedotransfer model with improved estimates of hydraulic parameter distributions and summary statistics (Rosetta3). J. Hydrol. 547, 39–53.
- Zhang, Y., Schaap, M.G., Zha, Y., 2018. A high-resolution global map of soil hydraulic properties produced by a hierarchical parameterization of a physically based water retention model. Water Resour. Res. 54, 9774–9790.
- Zhao, Y., Si, B., Zhang, Z., Li, M., He, H., Hill, R.L., 2019. A new thermal conductivity model for sandy and peat soils. Agr. Forest Meteorol. 274, 95–105.
- Weber, T.K.D., Weihermüller, L., Nemes, A., Bechtold, M., Degré, A., Diamantopoulos, E., Fatichi, S., Filipović, V., Gupta, S., Hohenbrink, T.L., Hirmas, D.R., Jackisch, C., Lier, Q. de J. van, Koestel, J., Lehmann, P., Marthews, T.R., Minasny, B., Pagel, H., Ploeg, M. van der, Svane, S.F., Szabó, B., Vereecken, H., Verhoef, A., Young, M., Zeng, Y., Zhang, Y., Bonetti, S., 2024. Hydro-pedotransfer functions: A roadmap for future development. Hydrol. Earth Syst. Sci. 28, 3391–3433.